# Effects of irradiation damage on the back-scattering of electrons: Silicon-implanted silicon

L Nasdala, A Kronz, D Grambole, Ghislain Trullenque

*American Mineralogist, Volume 92, pages 1768–1771, 2007*

LETTER

# Effects of irradiation damage on the back-scattering of electrons: Silicon-implanted silicon

LUTZ NASDALA,[1,*] ANDREAS KRONZ,[2] DIETER GRAMBOLE,[3] AND GHISLAIN TRULLENQUE[4]

[1]Institut für Mineralogie und Kristallographie, Universität Wien, A-1090 Wien, Austria
[2]Geowissenschaftliches Zentrum der Georg-August-Universität Göttingen, D-37077 Göttingen, Germany
[3]Forschungszentrum Dresden-Rossendorf, Institut für Ionenstrahlphysik und Materialforschung, D-01328 Dresden, Germany
[4]Institut für Geowissenschaften, Johannes Gutenberg-Universität, D-55099 Mainz, Germany

## ABSTRACT

Radiation damage in a (initially crystalline) silicon wafer was generated by microbeam ion implantation with 600 keV $Si^+$ ions (fluence $5 \times 10^{14}$ ions/cm$^2$). To produce micro-areas with different degrees of damage, 14 implantations at different temperatures (between 23 and 225 °C) were done. The structural state of irradiated areas was characterized using Raman spectroscopy and electron back-scatter diffraction. All irradiated areas showed strong structural damage in surficial regions (estimated depth <1 μm), and at implant substrate temperatures of below 130 °C, the treatment caused complete amorphization. Back-scattered electron (BSE) image intensities correlate with the degree of irradiation damage; all irradiated areas were higher in BSE than the surrounding host. Because there were no variations in the chemical composition and, with that, no $\overline{Z}$ contrast in our sample, this observation again supports the hypothesis that structural radiation damage may strongly affect BSE images of solids.

**Keywords:** Back-scattered electron images, Raman spectroscopy, electron back-scatter diffraction, radiation damage, silicon

## INTRODUCTION

In a recent study, Nasdala et al. (2006) described that structural radiation damage may notably increase the back-scattering of electrons and, thus, affect the grayscale patterns observed in back-scattered electron (BSE) images of single crystals. In that study, the BSE intensity of zircon ($ZrSiO_4$) single crystals correlated with the degree of accumulated self-irradiation damage, with the average atomic number (i.e., $\overline{Z}$ contrast) being less significant for the BSE. Their assertion was supported by the demonstration of how dry thermal annealing of the radiation damage, which was claimed to have only minor effects on the chemical composition, leads to a clear decrease of the mean back-scatter coefficient ($\overline{\eta}$). The authors attempted to explain their observation with decreased penetration depths of incident beam electrons in disordered structures, and assigned their observation as special case of electron channeling contrast.

In the meantime, not the interpretation but the observation has been questioned by several colleagues suspecting that the BSE intensity loss upon annealing might be due to changes in concentrations of elements that are not analyzed in the electron microprobe, such as loss of water. This aspect has already been discussed by Nasdala et al. (2006) who stated that if there was unrecognized loss of water, $\overline{Z}$, and, with that, the BSE intensity should increase, whereas the opposite was observed. On the other hand, it is clear that chemical changes of elements that are below the detection limit of the electron microprobe, or are not detectable, cannot be excluded from the outset.

In this paper, we present an unambiguous example for increased electron back-scattering caused by radiation damage. Structural damage has been produced by the local irradiation of a silicon wafer with silicon ions. This has produced a crystalline sample with several heavily damaged micro-areas, which uniformly consist of pure Si. Any $\overline{Z}$ contrast (Hall and Lloyd 1981; Lloyd 1987) can therefore be excluded in this case.

## SAMPLES AND EXPERIMENTAL DETAILS

A synthetic silicon sample, polished parallel to the crystallographic (100) plane, was implanted with 600 keV $Si^+$ ions. Irradiation experiments were done using the nuclear microprobe at the 3 MV tandetron accelerator of the Forschungszentrum Dresden-Rossendorf (Herrman and Grambole 1995). The sample chamber was evacuated to ~$10^{-8}$ mbar. To avoid notable ion channeling effects (e.g., Raineri et al. 1991; Dos Santos et al. 1995), the beam was irradiated with an angle of 7° to the surface normal. The beam was focused to a nearly square area 150 μm in size. The current density was 80 μA/cm$^2$, and the implantation fluence was $5 \times 10^{14}$ ions/cm$^2$. To produce areas with different degrees of damage, 14 irradiation experiments under identical conditions but at different temperatures were done. In doing this, we used the well-known fact that the amorphization rate of ion-beam irradiated solids depends strongly on temperature (e.g., Wang et al. 1998a, 1998b). To avoid any damage annealing upon re-heating, experiments were done beginning with the highest temperature (225; 200, between 180 and 100 °C at 10° steps; 80; 34; 23 °C). Implanted areas were placed in a row with separations of 0.3 mm. Considering the high thermal conductivity of silicon and the small size of the focal-spot area, local heating of the sample as a result of the implantation is negligible (compare Melngailis 1987).

Micro-Raman measurements were done with a Renishaw RM1000 spectrom-

* E-mail: lutz.nasdala@univie.ac.at

0003-004X/07/0010–1768$05.00/DOI: 10.2138/am.2007.2648 

eter equipped with Leica DMLM optical microscope, edge filter, a grating with 1200 grooves/mm, and Peltier-cooled CCD detector. Spectra were excited with the 632.8 nm emission (8 mW) of a He-Ne laser. Wavelength calibration was done using Ne lamp emissions. The wavenumber accuracy was better than 0.5 $cm^{-1}$ and the spectral resolution was determined at 2.2 $cm^{-1}$.

Electron back-scatter diffraction (EBSD) Kikuchi patterns (Baba-Kishi 1990) were obtained on a Zeiss DSM 962 scanning electron microscope (SEM) with W filament. The accelerating voltage was 20 kV. The sample stage was tilted ~70° relative to the surface normal and the free working distance was set to 19 mm. Patterns of manually selected micro-areas were obtained using a Nordlys detector coupled with the Channel5 computer package (HKL Technology ApS). Accumulation times were 15 s per point.

Back-scattered electron (BSE) imaging, as well as cathodoluminescence (CL) and secondary electron (SE) imaging, was done using a JEOL 8900 RL electron microprobe. To obtain BSE images, a paired semiconductor-type detector was operated in additive mode, then displaying "compositional atomic number contrast" with a sensitivity of better than 0.1 $\Delta$-$\bar{Z}$. The accelerating voltage was set to 25 kV and the beam current was chosen between 7 and 15 nA, measured on Faraday cup. Electron channeling patterns (ECP; Brooker et al. 1967; Wilkinson and Hirsch 1997) were obtained using the so-called pseudo-Kikuchi technique. Here, the electron beam rocks across a comparably large sample area while scanning under a low magnification (40×). This results in numerous angles (up to 4.29°) of the electron irradiation directions with respect to the surface normal, leading to variations of the total intensity of back-scattered electrons. For details see Brooker et al. (1967) and Baba-Kishi (2002). Prior to SEM-EBSD analysis and electron microprobe imaging, the sample was coated with a 150 Å thick carbon layer to avoid potential charging effects. Ultrapure carbon (less than 2 ppm impurities) was used for this, and the coating thickness was controlled with a Cressington MTM 10 oscillating quartz crystal detector.

## Characterization of the irradiation damage

We used Raman spectroscopy (Fig. 1A) to study the degree of damage produced in the sample by irradiation with 600 keV $Si^+$ ions. Structural damage was already studied in a nuclear microprobe using the micro Rutherford back-scatter (RBS)/Channeling technique, which uses changes in the stopping and back-scattering behavior of incoming ions to probe structural changes in the target; procedure and results have been described elsewhere (Grambole et al. 2007). Raman and RBS/Channeling spectra obtained in micro-areas that were implanted at temperatures below 140 °C (Raman) and 130 °C (RBS/Channeling), respectively, indicate complete amorphization. This is also seen from EBSD patterns (Fig. 2D); the absence of Kikuchi lines and bands indicates the complete loss of crystal order. Micro-areas implanted at temperatures of 130/140 °C and higher show gradually lower degrees of damage, however, significant irradiation damage (i.e., partial amorphization) is observed in all implantation areas up to 225 °C.

Monte Carlo simulations using the SRIM-2006 code (see Ziegler et al. 1985) predicted that irradiation with 600 keV $Si^+$ ions has damaged the Si target in a surficial layer of only ~1 µm thickness, with the maximum density of vacancies generated through atomic displacements in the depth range 550–800 nm. We have observed that bands of crystalline Si are fully absent in Raman spectra of micro-areas that were implanted at temperatures of 130 °C and below (i.e., the underlying host wafer does not contribute to the Raman scattered light). This is explained by the low penetration depth of visible light in amorphous silicon. In fact, for amorphous Si the depth probed by Raman spectroscopy with 6328 Å excitation is close to 140 nm (De Wolf et al. 1998). In contrast, with the RBS/Channeling technique the entire damaged layer is probed.

Raman spectra indicate that probed surficial layers of micro-areas irradiated at elevated temperatures in the range 140–225 °C consist of remnants of crystalline Si in a (dominating) volume fraction of amorphous Si. Amorphous fractions $f_A$ were determined from Raman spectra to quantify the structural damage. Two estimates based on the area integral of the LO=TO band (at ~521 $cm^{-1}$) of remnant crystalline Si, and the ratio of integrated Raman intensities in the wavenumber ranges 100–190 $cm^{-1}$ (amorphous dominant) and 920–1000 $cm^{-1}$ (crystalline dominant; see Fig. 1A), gave the same crystalline-to-amorphous ratios within an error of ±1.5%. However, amorphous fractions calculated from RBS/Channeling (Grambole et al. 2007) and Raman spectra show notable differences for most partially amorphized micro-areas (Fig. 1B). We explain this by the consideration that the two micro-techniques probe different sample depths.

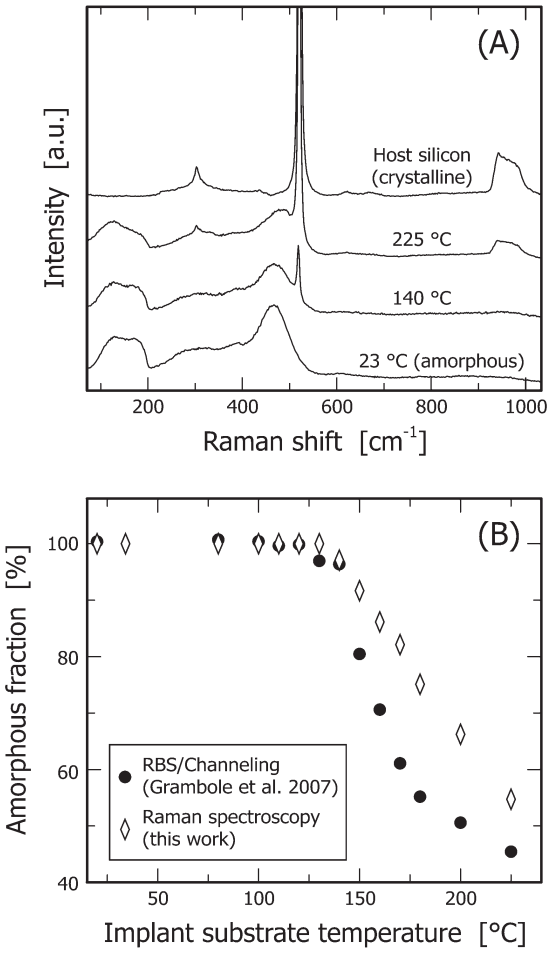


**Figure 1.** Analytical characterization of structural damage in $Si^+$-implanted silicon. (**A**) Raman spectra (stacked) of the same four areas as above. (**B**) Plot of the amorphous fraction calculated from RBS/Channeling and Raman spectra vs. the implantation temperature.

## Back-scattered electron imaging

A BSE image of the Si-implanted silicon wafer is presented in Figure 2A. The host wafer itself did not yield uniform BSE brightness, as it would correspond to its uniform chemical composition and structural state; rather it shows a blurred but

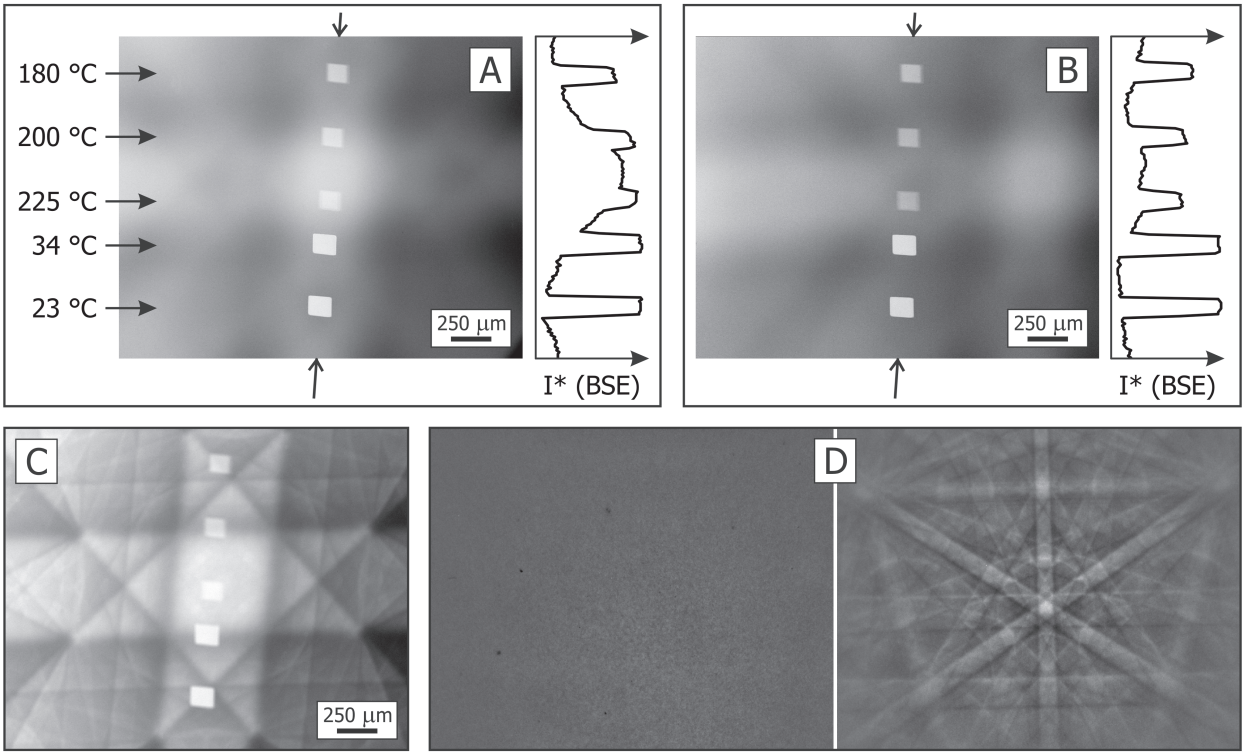


**FIGURE 2.** Electron microprobe and SEM images. (**A**) Back-scattered electron image of the silicon wafer. Five of the $Si^+$-implanted areas are seen as slightly distorted, bright rectangles. Implantation temperatures are quoted at the left side. I* = arbitrary grayscale values along the line marked with arrows. (**B**) Back-scattered image and grayscale plot of the same area after sample tilt. (**C**) Electron channeling (or pseudo-Kikuchi) pattern of the same area. The sample position (tilt) corresponds to **A**, i.e., view roughly along [100]. (**D**) An EBSD pattern obtained in the micro-area implanted at 80 °C (left) does not show any indication of diffraction (Kikuchi bands and lines are not seen) and, thus, it indicates amorphization. The corresponding EBSD pattern of the neighboring host (same experimental conditions; view roughly along [111]) is shown right.

somehow regular pattern of slightly brighter and darker patches. The phenomenon is related to the diffraction of back-scattered electrons. To verify this, an ECP (in early papers described as pseudo-Kikuchi or Kikuchi-like pattern) of the same area as shown in Figure 2A was obtained (Fig. 2C). This image suggests that the patchy appearance of the host silicon in Figure 2A can be described as an overlay of the "regular" BSE with a fuzzy Kikuchi pattern. The latter exhibits fourfold symmetry, which corresponds to the irradiation direction of the electron beam close to the [100] axis. The ECP (Fig. 2C) is not equivalent to the EBSD Kikuchi pattern (right part of Fig. 2D), even though both have been obtained from the same wafer. The EBSD pattern exhibits threefold symmetry because tilting the sample prior to SEM analysis has brought the [111] zone axis close to the center of the observation direction. Back-scattered electron images of geological samples are normally not affected by pseudo-Kikuchi patterns, because regular mechanical polishing does not produce surfaces whose quality is sufficient to observe these diffraction features.

The BSE image (Fig. 2A) shows five (out of a total of 14) irradiated micro-areas, which are easily recognized as bright, slightly distorted rectangular spots. This observation indicates that irradiation damage causes a significant increase of the back-scatter coefficient. The BSE intensity of partially amorphized areas (i.e., those that have been implanted at elevated temperatures) correlates inversely with the implantation temperature and, thus, it correlates with the degree of damage. The area irradiated at 225 °C (which represents the lowest degree of damage; Fig. 1B) shows the lowest BSE intensity among all implantation areas seen in Figure 2A, however, even this spot appears significantly brighter than the neighboring, undamaged host wafer. Areas implanted at low temperatures (i.e., those that have experienced complete surficial amorphization) are exceptionally high in BSE (see two spots closest to the bottom of Fig. 2A).

Monte Carlo simulations using the electron trajectory simulation program CASINO v. 2.42 (for the theoretical background see Newbury and Myklebust 1995) were done to estimate sampling depths of BSE images. For an accelerating voltage of 25 kV, results predicted that only ~44.2% of detected electrons are back-scattered from a depth shallower than 1 µm whereas more than 50% of detected electrons are back-scattered from the depth range between 1 and 2 µm. We may therefore speculate that observed BSE differences between irradiated areas and host wafer would have been even more pronounced if damaged layers had thicknesses >1 µm.

Neither SE nor CL images of the same areas showed notable differences in signal intensity among implantation spots and host wafer. This excludes the possibility that high BSE intensities of implantation areas are due to enhanced quantities of secondary electrons and/or luminescence emission that, as analytical arti-

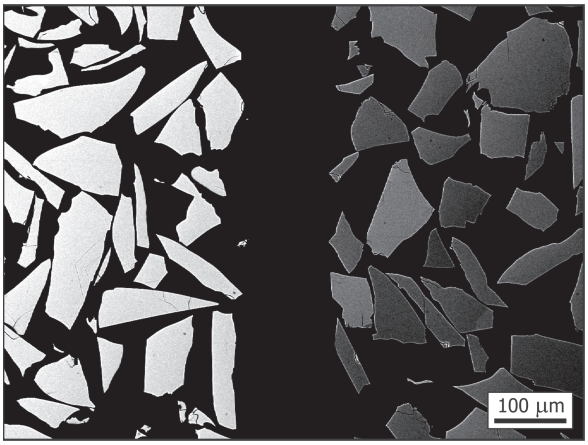


**FIGURE 3.** Back-scattered electron image of $SiO_2$. The sample consists of randomly oriented chips of $SiO_2$ glass (left) and α-quartz (right) embedded in epoxy. The BSE intensity of the glass is generally higher than that of quartz.

fact, have been registered by the BSE detector.

It might be speculated that the enhanced electron back-scattering of radiation-damaged phases is related to their lower density. However, CASINO simulations predicted that a target's density has insignificant effects on $\overline{\eta}$. Furthermore, it needs to be discussed critically whether the observed lower BSE intensity of the host crystal, when compared to the partially or fully amorphized implantation areas, might be simply due to crystal orientation contrast (Lloyd 1987), i.e., caused by enhanced channeling of incident beam electrons into the sample along [100]. If this was the case, the BSE intensity of the wafer should dramatically increase, and BSE differences between implanted areas on the one hand and host wafer on the other hand should decrease, after tilting the wafer. However, tilting the wafer a few degrees (Fig. 2B) caused insignificant changes in observed BSE intensities. This observation implies that different crystal orientations are less significant for the BSE than structural differences between a crystal and its amorphous analog. A similar observation is made when comparing the BSE intensities of $SiO_2$ glass and α-quartz (Fig. 3). The latter always yields lower BSE, with comparably minor BSE differences among α-quartz crystals with different orientations (i.e., the BSE phase contrast between crystalline and amorphous clearly exceeds the extent of the BSE crystal orientation contrast within the crystalline phase).

These observations imply that in the case of a randomly oriented crystalline target, compared to its amorphous analog, fewer electrons are back-scattered and/or back-scattered electrons have lower energies (recall that integral electron energies, not numbers of electrons, are registered by the BSE detector). This might be explained by the consideration that in crystalline materials, electrons penetrate on average deeper into the sample (for instance, along lattice planes after low-angle deflection). A sound interpretation, however, cannot be given at the present stage.

Our study reconfirms the observations of Nasdala et al. (2006); radiation-damaged solids do show higher BSE than their crystalline analogs. This structural effect, however, is probably only of importance in BSE imaging if single crystals show only minor internal $\overline{Z}$ contrast. To sort out the causes of the decreased penetration and absorption and the increased back-scattering of electrons of radiation-damaged and other amorphous/disordered phases, more systematic studies are needed.

## ACKNOWLEDGMENTS

We are indebted to T. Váczi for experimental assistance and to B. Griffin for stimulating discussions. Constructive reviews of F. Corfu and an anonymous expert are gratefully acknowledged. Partial funding of this research was provided by the European Commission through contract no. MEXC-CT-2005-024878 and Research Infrastructures Transnational Access (RITA) contract no. 025646.

## REFERENCES CITED

Baba-Kishi, K.-Z. (1990) A study of directly recorded RHEED and BKD patterns in the SEM. Ultramicroscopy, 34, 205–218.

——— (2002) Electron backscatter Kikuchi diffraction in the scanning electron microscope for crystallographic analysis. Journal of Materials Science, 37, 1715–1746.

Brooker, G.R., Shaw, A.M.B., Whelan, M.J., and Hirsch, P.B. (1967) Some comments on the interpretation of the "Kikuchi-like reflection patterns" observed by scanning electron microscopy. Philosophical Magazine, 16, 1185–1191.

De Wolf, I., Jiménez, J., Landesmann, J.-P., Frigeri, C., Braun, P., Da Silva, E., and Calvet, E. (1998) Raman and luminescence spectroscopy for microelectronics. Catalogue of optical and physical parameters. "Nostradamus" project SMT4-CT-95-2024. Office for Official Publications of the European Communities, Luxembourg.

Dos Santos, J.H.R., Grande, P.L., Boudinov, H., Behar, M., Stoll, R., Klatt, C., and Kalbitzer, S. (1995) Electronic stopping power of ⟨100⟩ axial-channelled He ions in Si crystals. Nuclear Instruments and Methods in Physics Research B, 106, 51–54.

Grambole, D., Herrmann, F., Heera, V., and Meijer, J. (2007) Study of crystal damage by ion implantation using micro RBS/Channeling. Nuclear Instruments and Methods in Physics Research B, 260, 276–280.

Hall, M.G. and Lloyd, G.E. (1981) The SEM examination of geological samples with a semiconductor back-scattered electron detector. American Mineralogist, 66, 362–368.

Herrmann, F. and Grambole, D. (1995) The new Rossendorf nuclear microprobe. Nuclear Instruments and Methods in Physics Research Section B: Beam Interactions with Materials and Atoms, 104, 26–30.

Lloyd, G.E. (1987) Atomic number and crystallographic contrast images with the SEM: a review of backscattered electron techniques. Mineralogical Magazine, 51, 3–19.

Melngailis, J. (1987) Focused ion beam technology and applications. Journal of Vacuum Science and Technology B: Microelectronics and Nanometer Structures, 5, 469–495.

Nasdala, L., Kronz, A., Hanchar, J.M., Tichomirowa, M., Davis, D.D., and Hofmeister, W. (2006) Effects of natural radiation damage on back-scattered electron images of single-crystals of minerals. American Mineralogist, 91, 1738–1746.

Newbury, D.E. and Myklebust, R.L. (1995) NIST Micro MC: A user's guide to the NIST microanalysis Monte Carlo electron trajectory simulation program. Microbeam Analysis, 4, 165–175.

Raineri, V., Galvagno, G., Rimini, E., Biersack, J.P., Nakagawa, S.T., La Ferla, A., and Carnera, A. (1991) Channelling implants of B ions into ⟨100⟩ silicon surfaces. Radiation Effects and Defects in Solids, 116, 211–217.

Wang, L.M., Wang, S.X., Gong, W.L., and Ewing, R.C. (1998a) Temperature dependence of Kr ion-induced amorphization of mica minerals. Nuclear Instruments and Methods in Physics Research B, 141, 501–508.

Wang, L.M., Wang, S.X., Gong, W.L., Ewing, R.C., and Weber, W.J. (1998b) Amorphization of ceramic materials by ion beam irradiation. Materials Science and Engineering, A253, 106–113.

Wilkinson, A.J. and Hirsch, P.B. (1997) Electron diffraction based techniques in scanning electron microscopy of bulk materials. Micron, 28, 279–308.

Ziegler, J.F., Biersack, J.P., and Littmark. U. (1985) The Stopping and Range of Ions in Solids. Pergamon Press, New York.

MANUSCRIPT RECEIVED MARCH 22, 2007
MANUSCRIPT ACCEPTED MAY 29, 2007
MANUSCRIPT HANDLED BY BRYAN CHAKOUMAKOS